Solvent-assisted *in situ* synthesis of cysteamine-capped silver nanoparticles

View the article online for updates and enhancements.

Related content

Solvent-assisted *in situ* synthesis of cysteamine-capped silver nanoparticles

José M Oliva[1]**, Julio M Ríos de la Rosa**[1,2]**, María J Sayagués**[3]**,
José A Sánchez-Alcázar**[4]**, Patrick J Merkling**[1] **and Ana P Zaderenko**[1]

[1] Departamento de Sistemas Físicos, Químicos y Naturales, Área de Química-Física, Universidad Pablo de Olavide, ES-41013 Seville, Spain
[2] NorthWest Centre of Advanced Drug Delivery, University of Manchester, M139PT Manchester, United Kingdom
[3] Instituto de Ciencia de Materiales de Sevilla (CSIC-US), ES-41092 Seville, Spain
[4] Centro Andaluz de Biología del Desarrollo, ES-41013 Seville, Spain

E-mail: apzadpar@upo.es

CrossMark

Abstract

Silver nanoparticles offer a huge potential for biomedical applications owing to their exceptional properties and small size. Specifically, cysteamine-capped silver nanoparticles could form the basis for new anticancer therapies combining the cytotoxic effect of the silver core with the inherent antitumor activity of cysteamine, which inhibit cancer cell proliferation and suppress invasion and metastasis. In addition, the capability of the cysteamine coating monolayer to couple a variety of active principles and targeting (bio)molecules of interest proves key to the tailoring of this platform in order to exploit the pathophysiology of specific tumor types. Nevertheless, the chain length and conformational flexibility of cysteamine, together with its ability to attach to the surface of silver nanoparticles via both the thiol and the amine group, have made the *in situ* synthesis of these particles an especially challenging task. Herein we report a solvent-assisted *in situ* synthesis method that solves this problem. The obtained nanoparticles have been fully characterized by UV–visible absorption spectroscopy, Fourier transform infrared spectroscopy, transmission electron microscopy, electron diffraction measurement, high resolution transmission electron microscopy, scanning transmission electron microscopy, energy dispersive x-ray spectroscopy nanoanalysis, and dynamic light scattering measurement. Our synthesis method achieves extremely high yield and surface coating ratio, and colloidal stability over a wide range of pH values including physiological pH. Additionally, we have demonstrated that cysteamine-capped nanoparticles obtained by this method can be conjugated to an antibody for active targeting of the epidermal growth factor receptor, which plays an important role in the pathogenesis and progression of a wide variety of tumors, and induce cell death in human squamous carcinoma cells. We believe this method can be readily extended to combinations of noble metals and longer chain primary, secondary, ternary or even quaternary aminethiols.

Keywords: cysteamine, 2-mercaptoethylamine, silver nanoparticles, DMF, targeted antitumor therapy, epidermal growth factor receptor
Classification numbers: 2.03, 4.02

S Supplementary material for this article is available online

1. Introduction

Noble metal nanoparticles offer a huge potential for biomedical applications due to their exceptional properties and their ability to be coupled to molecules and biomolecules of interest [1–10]. For this purpose, the most common strategy is to functionalize their surface with chemical groups allowing for subsequent coupling via self-attachment of suitable thiol monolayers on the growing nuclei, i.e. *in situ* synthesis [2–4]. In this sense, short-chain thiols such as cysteamine (2-mercaptoethylamine) represent an optimal choice for functionalization because they do not increase particle size significantly, which is critically important for most biomedical applications.

Although an *in situ* synthesis of cysteamine-capped silver nanoparticles has been described [11], the initial metal concentrations required to obtain nanoparticles are extremely low and it has not been widely used so far. These initial low concentrations, which translate into low nanoparticle concentrations, might be suitable for sensing applications [11, 12], but may be too low for most biomedical formulations. Therefore, achieving an *in situ* synthesis of stable cysteamine-capped silver nanoparticles at high nanoparticle concentrations is highly desirable and still remains a scientific challenge.

Cysteamine is a short chain thiol approved by the Food and Drug Administration (FDA) for the treatment of cystinosis that stands out for its broad range of applications not only in the biomedical field, with potential use in the treatment of malaria, acquired immunodeficiency syndrome, Huntington's disease, or cancer, among others [13]. When coupled to nanoparticles, cysteamine can also act as a linker both in drug delivery vectors [14–22] and in bio- and chemical-sensors [23–31]. With regard to its anticancer activity, cysteamine has been proved to prevent metaplasia and carcinogenesis induced by radiation or chemicals [32–34], to inhibit cancer cell proliferation [35], to suppress invasion and metastasis [36], and to induce autophagy in cancer cells [37]. Moreover, a wide range of nanoparticles functionalized with cysteamine have in fact shown antitumor activity [38–42], yet none of these are made up of silver despite being a cytotoxic material of choice. Indeed, the toxicity of silver nanoparticles has been widely explored in the context of bactericidal agents owing to their potential to overcome antibiotic resistance, and is now extending its potential to the development of new cancer therapies [43]. Like any other chemotherapeutic cytotoxic agent, silver should be vectorized to the tumor cells to avoid adverse effects on healthy tissues. In this sense, cysteamine offers the advantage of acting as a linker between the silver nanoparticle and the targeting agent, providing a coating layer on the surface of the nanoparticle made up by amino groups able to ensure the orientational binding of targeting antibodies, while providing the nanocarrier with additional and valuable antitumor properties.

In this work we report a new method for the *in situ* synthesis of cysteamine-capped silver nanoparticles. Our synthesis method achieves a high yield, an extremely high surface coating, and exceptional colloidal stability. An additional layer of complexity was introduced by conjugating an antibody to target silver nanoparticles to cancer cells overexpressing the epidermal growth factor receptor (EGFR), a 'hot' target protein that plays an important role in the pathogenesis and progression of a wide variety of tumors.

2. Experimental

Silver nitrate, N,N-dimethylformamide (DMF) and 2-(N-morpholino)ethanesulfonic acid (MES) were purchased from Panreac. Sodium borohydride ($NaBH_4$) was purchased from Sigma-Aldrich. 2-Mercaptoethylamine hydrochloride (cysteamine), (N-(3-dimethylaminopropyl)-N′-ethylcarbodiimide hydrochloride (EDC) and N-hydroxysuccinimide (NHS) were purchased from Alfa Aesar. Anti-EGFR (528) AF488 sc-120 (Ab) was purchased from Santa Cruz Biotechnology. Water was purified using a milli-Q (18.2 MΩ) reagent-grade water system from Millipore. Dialysis membranes Cellu Sep T3 (12–14 kDa) were supplied from Membrane Filtration Products, Inc. Prior to synthesis, all glassware was cleaned with aqua regia.

2.1. Synthesis of nanoparticles

Cysteamine-capped silver nanoparticles (Ag@cys) were synthesized by reduction of silver nitrate in the presence of cysteamine as capping agent, and DMF as reaction medium. In a typical preparation, 500 μl of an aqueous solution of cysteamine (0.7 mmol) and 500 μl of an aqueous solution of $AgNO_3$ (0.234 mmol) were sequentially added to 20 ml of DMF, as reaction medium, under stirring in an ice bath. Afterwards, 3 ml of an aqueous solution of $NaBH_4$ (210 mM) were added dropwise. The reaction mixture was stirred for 20 min, after which Ag@cys nanoparticles were recovered by centrifugation (8000 rpm, 10 min), resuspended in 20 ml MES buffer (50 mM) and purified by dialysis against water for 48 h. The resulting nanoparticles were then lyophilized to obtain 21.2 ± 0.4 mg of Ag@cys as a dark brown powder. The reaction yield, calculated as the amount of Ag^+ in the recovered nanoparticles with respect to the initial amount of Ag^+ in the reaction, was 79%.

To determine the pH range in which Ag@cys nanoparticles are stable, a set of nanoparticles was dispersed in water (1 mg ml^{-1}) and the pH modified from pH 2 to 10 by adding appropriate amounts of an aqueous solution of NaOH (0.1 M) or HCl (0.1 M).

To obtain cysteamine-capped silver nanoparticles targeted to the epidermal growth factor receptor (EGFR), a set of Ag@cys nanoparticles was conjugated to a monoclonal antibody to EGFR through carbodiimide-based chemistry, according to a protocol previously developed by our group to ensure the correct steric orientation of the targeting antibody on the nanoparticle surface [44]. Briefly, a mixture of 250 μl Ag@cys (1 mg ml^{-1}, in 50 mM MES, pH 6.5), 250 μl EDC (5.2 mM in 50 mM MES, pH 6.5) and 2.5 ml NHS (8.7 mM in 50 mM MES, pH 6.5) was stirred at room temperature for 30 min. Afterwards, 250 μl of anti-EGFR (50 μg ml^{-1}) were

Adv. Nat. Sci.: Nanosci. Nanotechnol. **9** (2018) 015001

J M Oliva *et al*

added and the mixture stirred for 24 h. The resulting suspension of targeting nanoparticles, namely Ag@cys@Ab, was centrifuged at 6000 rpm in order to wash off excess unbound antibody and coupling reagents. The nanoparticles were then resuspended in a BSA 0.1% (w/v) solution (in milli-Q water) and stored at 4 °C until their use in biological assays.

2.2. Characterization

Ag@cys nanoparticles were characterized by UV–vis absorption spectroscopy, Fourier transform infrared (FTIR) spectroscopy, transmission electron microscopy (TEM), electron diffraction (ED) measurement, high resolution transmission electron microscopy (HRTEM), scanning transmission electron microscopy (STEM), energy dispersive x-ray (EDX) spectroscopy nanoanalysis and dynamic light scattering (DLS) measurement. FTIR spectra were recorded on a Bruker IFS 66/s spectrometer equipped with a DTS detector. We averaged 150 scans with a scan frequency of 2.5 Hz and 3 cm^{-1} resolution. The samples were prepared by depositing 100 μl of an aqueous suspension of nanoparticles on a silicon plate. The as prepared samples were allowed to dry at room temperature before recording the spectra. UV–vis spectra were recorded on an Ocean optics spectrometer equipped with a HR4000 detector with quartz cuvette of 1 cm optic pass. One milliliter of the nanoparticles suspension was added to the quartz cuvette. TEM images and ED patterns were performed on a 200 kV Philips CM200 microscope equipped with a supertwin objective lens and a LaB6 filament (point resolution 0.25 nm). The samples were prepared by drying a drop of an aqueous suspension of nanoparticles on a carbon coated copper grid. HRTEM and STEM images were obtained with a high-angle annular dark field (HAADF) detector in a 300 kV TECNAI G2 F30 microscope with a field emission system (point resolution 0.2 nm). The samples were prepared by drying a drop of an aqueous suspension of nanoparticles on a carbon coated copper grid. EDX nanoanalysis was performed in STEM mode and the analysis of the spectra and the HAADF-STEM images were done with the ES vision software (FEI Company). The samples were prepared by drying a drop of an aqueous suspension of nanoparticles on a carbon coated copper grid. Hydrodynamic diameter and zeta potential were measured on a Zetatrac (Microtrac). Two milliliters of the nanoparticle suspension were added to the cavity and measured by DLS at room temperature (25 °C).

2.3. Cellular cytotoxicity and uptake assays

The biological behavior of nanoparticles was evaluated in the A431 human squamous carcinoma cell line, an epidermoid carcinoma target model to study the effect of therapeutic approaches directed to EGFR owing to the overexpression of this protein. Cells were cultured in roswell park memorial institute (RPMI) medium supplemented with 10% fetal bovine serum (FBS) and 50 U ml^{-1} penicillin/streptomycin, and grown at 37 °C and 5% (v/v) CO$_2$.

Cytotoxicity was evaluated using the *in vitro* Toxicology Assay Kit, Resazurin based (Sigma-Aldrich), according to the kit specifications, after inoculating cells with growing amounts of nanoparticles (5–100 μg ml^{-1}, final concentration). The cell viability was expressed as a relative percentage compared to untreated cells and all results were expressed as mean $\pm$ standard deviation (SD). The student's *t*-test was used to analyze the data and statistically significant differences. Only *p*-values smaller than 0.05 were considered as statistically significant. For cell uptake visualization, A431 cells were grown on 1 mm (goldseal no.1) glass coverslips for 48 h in RPMI medium, supplemented as described above. At this stage cells were rinsed with phosphate-buffered saline (PBS), inoculated with culture medium containing 10 μg ml^{-1} of nanoparticles and cultured for 2 h, rinsed with PBS and cultured during 48 h in fresh culture medium. Cells were then rinsed once with PBS, fixed in 4% (w/v) paraformaldehyde (PFA) for 5 min at room temperature (25 °C), and permeabilized in 0.1% (w/v) saponin in PBS for 5 min. Cells were subsequently stained with Hoechst 33342 (1 mg ml^{-1}) and washed with PBS. The presence of silver nanoparticles and anti-EGFR was analyzed by dark field and fluorescence microscopy, respectively, using a Leica DM 2500 microscope (lens: 100$\times$ oil).

3. Results and discussion

3.1. Synthesis and characterization of cysteamine-capped silver nanoparticles

We have accomplished the *in situ* syntheses of cysteamine-capped silver nanoparticles by reducing silver nitrate in the presence of cysteamine in two different reaction media, water and DMF. Both selected solvents are polar, according to the polar nature of the reactants, but while the first is protic, the second is aprotic. The reduction was performed using a strong reducing agent, sodium borohydride, and a cysteamine:Ag ratio that could be held as low as 3:1 in DMF. This compares favorably to the water case described in the literature [11], in which ratios of 40:1 were used. Additionally, another advantage of DMF is that the synthesis in DMF has long-term stability, and is reproducible. Attempts to synthesize stable cysteamine-capped silver nanoparticles in aqueous medium at a cysteamine:Ag ratio of 3:1 failed, as shown by the absence of the characteristic silver nanoparticle plasmon in the UV–vis spectrum (figure 1). Instead, nanoparticles grow out of control due to Ostwald ripening and the sample turns grey immediately after the addition of the reducing agent, which indicates the formation of large particles of metallic silver (inset of figure 1).

The strong background absorption in the UV–vis spectrum provides further evidence for this growth. Thus, cysteamine fails to stabilize nanoparticles during the growth step in aqueous medium resulting in aggregation. Contrary to what happens when using water as reaction medium, Ag nanoparticles synthesized in DMF exhibit a strong plasmon peaking
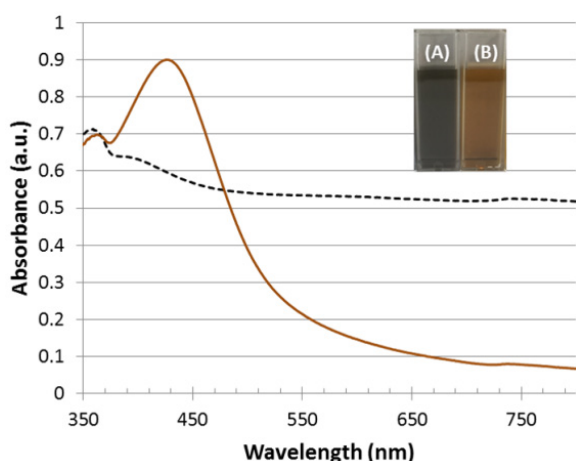
Figure 1. Absorption spectra of products obtained using water (dashed line) or DMF (solid line) as solvent for the synthesis of cysteamine-capped nanoparticles, after purification. Inset: digital photographs of the colloidal suspensions obtained using aqueous medium (A) or DMF (B) as solvent.
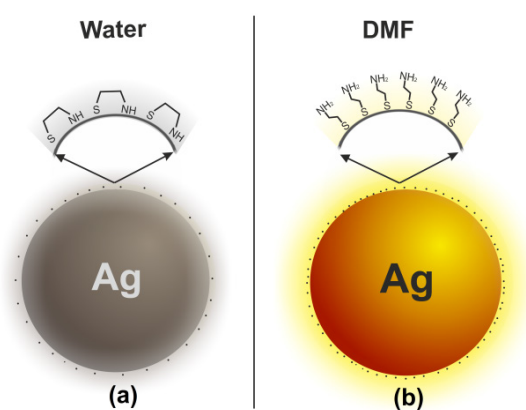

Figure 2. Schematic representation of cysteamine-capped silver nanoparticles with cysteamine in gauche (a) and trans (b) conformations.

at 426 nm (figure 1), which is characteristic of silver nanoparticles and indicates that this solvent yields nanoparticles. Therefore, all subsequent characterization techniques were applied to the nanoparticles obtained using DMF as solvent, hereinafter Ag@cys. The fact that the synthesis is successful in DMF but not in water can be explained based on the nature of both the ligand and the solvent. It has been described that cysteamine is able to bind to the surface of silver through both the thiol and the amine group (figure 2(a)) [45]. This bidentate linkage necessarily leads to a decrease of the coating degree, a decrease in surface groups and charge, and consequently to a decrease in the stability of the nanoparticles. According to our results, DMF, as a polar aprotic solvent that stabilizes cationic species such as the positively charged amine group of cysteamine hydrochloride, hinders its interaction with the nanoparticle surface and promotes the interaction of the ligand through the thiol group (figure 2(b)), resulting in increased coating, as discussed later. Additionally, another remarkable advantage of our *in situ* synthesis versus ligand exchange or ligand addition after the synthesis, is that the presence of the

reducing agent in the reaction medium prevents the formation of disulfide bridges initially present or that might form in atmospheric conditions, eliminating the need to carry out the functionalization of nanoparticles under inert atmosphere [46].

Taking into account that the stability of metal nanoparticles depends to a great extent on the ionization state of their surface coating, the stability of Ag@cys nanoparticles should be influenced by the net charge of the amine layer on their surface and, therefore, by the pH of the dispersing medium. Amine groups are positively charged at low pH; but the higher the pH, the more uncharged groups are present, and these are able to form hydrogen bonds between nanoparticles inducing their aggregation. The exact value at which this takes place depends on the effective pK_a of the nanoparticles, i.e. the pH value at which half of the groups are protonated. This value is, as a general rule, significantly lower than that of the free ligand [47]. To determine the pH range in which our colloid is stable and no aggregation occurs, nanoparticles were dispersed in water and the pH set to values from pH 2 to 10. The stability was evaluated in terms of surface plasmon by UV–vis absorption spectrophotometry (figure 3). As can be seen in figure 3, Ag@cys nanoparticles are stable over a wide pH range. From pH 2 to 5 nanoparticles are well dispersed, as revealed by a narrow plasmon, and at pH 6–7 nanoparticles get closer but no aggregation takes place, as shown by a lower plasmon absorbance at 426 nm while an increase in absorbance is observed in the 600 nm region. At pH 8, the increase in absorbance in the 600 nm region turns into a band owing to the coupling of adjacent dipolar plasmons [46], as a consequence of the lower amount of charged amino groups at this pH. At even higher pH values, the net charge is lost completely and nanoparticles aggregate and precipitate out of the solution, as can be seen from the absence of an absorption peak in the plasmon region. Our nanoparticles can therefore be used over a fairly ample pH range that includes physiological pH.

The surface modification of nanoparticles with cysteamine was also analyzed by Fourier transform infrared (FTIR) spectroscopy and transmission electron microscopy (TEM). The comparison between the FTIR spectra of the dialyzed Ag@cys nanoparticles and cysteamine hydrochloride (figure 4) demonstrates the proper surface functionalization of Ag nanoparticles with cysteamine: the disappearance of the characteristic SH stretching vibration at 2598 cm^{-1} in Ag@cys proves that the thiol group binds to the nanoparticle surface through the sulfur atom. Furthermore, while this vibration is still present in Ag@cys prior to the nanoparticle purification process due to the excess of unreacted cysteamine hydrochloride in the reaction medium, it disappears following dialysis (figure S1 in supplementary (stacks.iop.org/ANSN/9/015001/mmedia)). Additionally, the characteristic NH$_2$ bending vibration at 1589 cm^{-1} remains in Ag@cys being, in fact, the strongest band in the spectrum.

The TEM analysis of Ag@cys nanoparticles revealed that they are spherical (figure 5(a)) and crystalline, and all the rings could be indexed in the cubic system of metallic silver (Fm3m, $a = 0.4$ nm; figure 5(b)). In the HRTEM micrograph
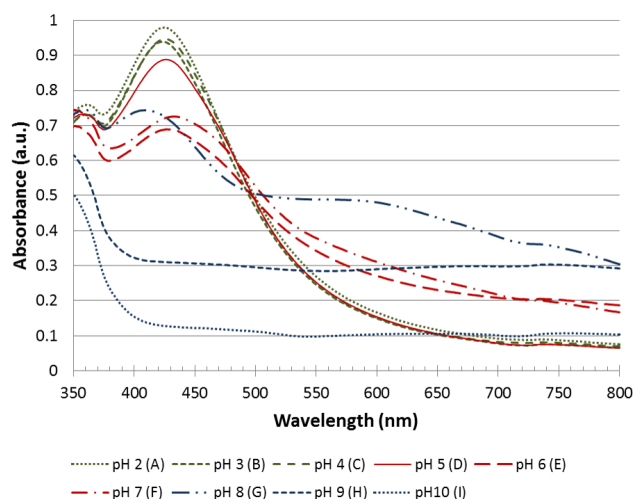
Figure 3. Absorption spectra of Ag@cys resuspended in water at different pH values.

Figure 4. Comparison between the FTIR absorbance spectra of dialyzed Ag@cys nanoparticles (black line) and cysteamine hydrochloride (blue line). The spectra are normalized with respect to the $1589\,cm^{-1}$ peak.

shown in figure 5(c) crystalline silver nanoparticles are clearly seen and the corresponding $(h\,k\,l)$ planes have been marked. Finally, figure 5(d) shows an enlargement of a silver nanoparticle oriented along (1 1 1).

Additionally, nanoparticle size was determined both by TEM and DLS. According to TEM, their average diameter is 12 nm, which is in good agreement with the hydrodynamic diameter obtained by DLS of 15 nm (figure S2 in supplementary). Moreover, their zeta potential is extremely high (36 mV at pH values up to 5, and remains around 30 mV up to pH 8), a fact that is in keeping with good long-term stability. Such a high value is also an indicator for a high surface coverage, as was confirmed by EDX. In contrast, the reported zeta potential for the *in situ* synthesis published in water is just 18.7 mV at pH 4 [12], a value far too low for biomedical applications (± 30 mV), and that necessarily worsens at higher pH values given that the zeta potential depends on the charge and the amino groups deprotonate at higher pH values. Additionally, if we analyze further our results in the light of the reported synthesis in water, we find that the initial silver concentration ($\sim 10^{-5}$ M [11]) is several orders of magnitude lower than the one achieved in our synthesis (0.012 M). Assuming that nanoparticles are spherical, as indicated by the TEM images, equation 1 may be applied [48]

$$C = \frac{c_{\mathrm{M}} M_{\mathrm{Ag}}}{\frac{4}{3}\pi r^3 \rho N_0},\qquad(1)$$

where c_{M} is the molar concentration of AgNO$_3$, M_{Ag} is the molar mass of silver, r is the average radius of nanoparticles, ρ is the density of silver (10.49 g cm^{-3}), and N_0 is Avogadro's number. This yields a concentration of silver nanoparticles of up to 7.6×10^{-10} M [11], assuming 100% yield. This compares to our value of 1.7×10^{-7} M that takes into account the yield of the reaction (79%), which means that our concentration of nanoparticles is at least 220 times higher than the one reported in water.

The chemical composition of Ag@cys nanoparticles was studied in detail by EDX analysis performed in HAADF-STEM mode, allowing quantification in very small regions
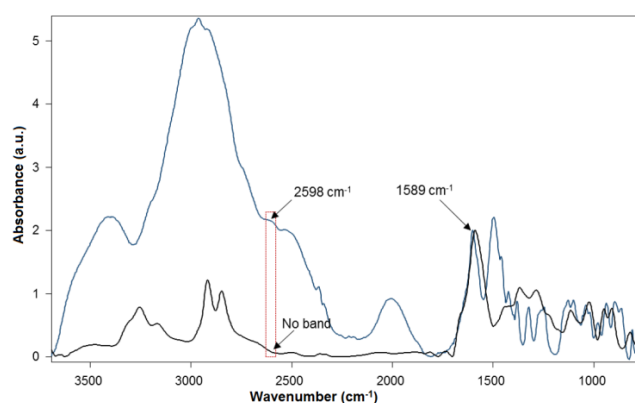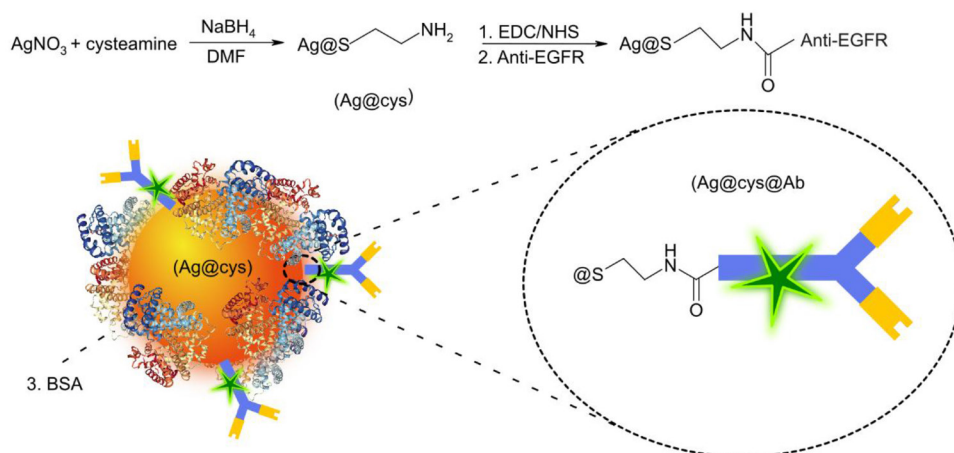
to obtain the Ag:S atomic ratio in the nanoparticles. Multiple spectra with the beam focused on different silver nanoparticles (figure 6(a)) were recorded to get a faithful representation of nanoparticle environments, and a representative spectrum is shown in figure 6(b). The average atomic percentage was found to be 90.5% silver and 9.5% sulfur.

To determine the Ag:S atomic ratio on the nanoparticle surface, an EDX spectrum profile analysis was done, and a representative result is shown in figure 7. Twenty spectra were recorded along the line profile observed in the HAADF-scanning image including edges and centers of three nanoparticles (figure 7(a)). The Ag and S profile composition is presented in figures 7(b) and (c), respectively, and their atomic percentages found at a selection of representative points are shown in table 1. Whereas the values at the center of the nanoparticles are very similar to the Ag:S ratio average, at the edges of the nanoparticles the sulfur percentage increases considerably, reaching values of more than 55%. By combining the imaging information with the chemical composition provided by this technique, it can be concluded that silver nanoparticles are capped with thiol molecules, in agreement with the results from FTIR.

Considering that for a particle size of 12 nm approximately 14% of silver atoms are on the surface, and taking into account that the average atomic percentage Ag:S in Ag@cys nanoparticles is 90.5:9.5, it is thus estimated that the cysteamine to surface silver ratio is 3:4, i.e. three cysteamine molecules for every four silver atoms on the metal surface of nanoparticles. This surface coverage is remarkably higher than that obtained for other *in situ* syntheses with other thiols, such as the widely employed tiopronin (a tiopronin molecule for every three silver atoms on the metal surface of nanoparticles) [49], and is in agreement with previous studies on gold showing that the self-assembly of cysteamine monolayers on the metal surface is more effective using DMF as solvent than water [50]. The surface coverage was calculated by the following equation with results summarized in table 2

$$\mathrm{CF} = \frac{S(\%)}{\text{Ag surface of nanoparticle}(\%)}.\qquad(2)$$

Figure 5. Microstructural characterization of Ag@cys nanoparticles: (a) TEM image; (b) EDX pattern; (c) and (d) HRTEM micrographs.

Figure 6. Compositional characterization of Ag@cys nanoparticles: (a) HAADF-STEM image showing the positions at which the EDX analysis has been done; (b) representative EDX spectrum and the average Ag:S atomic ratio averaged over all positions.

Figure 7. Ag:S profile analysis. (a) HAADF-STEM profile image exploring red and blue points at which the EDX analysis has been done along a straight line; (b) and (c) silver and sulfur profile composition, respectively, found by EDX analysis from left to right at the points highlighted in red and blue in (a).

Table 1. Ag and S atomic percentages found at a selection of representative points.

Point		2	4	6	8	10	12	15	17	19
Atomic percentage (%)	Ag	45.8	91.6	46.6	41.0	82.3	32.3	63.7	90.2	46.1
	S	55.2	8.4	53.4	59.0	17.7	67.6	36.3	9.8	53.9

As shown in table 2, the coverage fraction of cysteamine-capped silver nanoparticles obtained by our *in situ* synthesis method more than doubles that of the tiopronin-capped nanoparticles, providing increased coating. This is due largely, but not exclusively to the reduced bulkiness of cysteamine, as can be appreciated from figure S3 (in supplementary) showing the

Table 2. Ligand (*L*) coverage fraction (CF) of Ag@cys nanoparticles compared to Ag@tiopronin nanoparticles [49].

	L	CF
This work	Cysteamine	0.76
Castillo *et al* [49]	Tiopronin	0.33

Scheme 1. Schematic representation of cysteamine-capped silver nanoparticles functionalized with AlexaFluor488-labelled anti-EGFR antibody (Ag@cys@Ab) via carbodiimide-based chemistry (steps 1 and 2), and blockage of unspecific binding sites with BSA (step 3).

solvent-accessible volume. A projection perpendicular to the major component of the inertia axis of the molecule yields van der Waals areas of 17.9 $Å^2$ and 23.2 $Å^2$ for cysteamine and tiopronin, respectively. Moreover, the obtained cysteamine coverage means that the total yield of the synthesis as referred to the cost-limiting silver is remarkably high, 79%.

3.2. Biological behavior in epidermoid carcinoma cells

New antitumor therapies focus on the targeting of chemotherapeutic agents to tumor cells to avoid side effects in healthy tissues. To assess whether our nanoparticles can be vectorized to specific targets of biomedical interest in cancer therapy, a set of nanoparticles was conjugated to an antibody to EGFR. We have chosen this receptor because of its relevance in current antitumor treatments. EGFR is a transmembrane glycoprotein with tyrosine kinase activity, which is involved in the regulation of cellular proliferation, differentiation, and survival, playing an important role in the pathogenesis and progression of a wide variety of tumors such as gliomas and carcinomas of the lung, colon, head and neck, pancreas, ovary, breast, bladder, and kidney. For this reason, this receptor has become a major target in cancer therapy, both in terms of specific inhibition [51–53] and vectorization [54]. A carbodiimide-mediated coupling reaction was used to conjugate the anti-EGFR antibody (Ab) to our cysteamine-capped silver nanoparticles. In this reaction, an amide bond is formed between the free amine groups of the cysteamine monolayer in Ag@cys and the carboxyl terminus of the antibody to yield Ag@cys@Ab (scheme 1), ensuring that the orientation of the antibody on the nanoparticle surface is appropriate for the interaction with its receptor, i.e. the paratope of the antibody remains free. A water-soluble carbodiimide, EDC, was used in tandem with NHS, to improve the water stability of the carboxylic acid-activated intermediate [44].

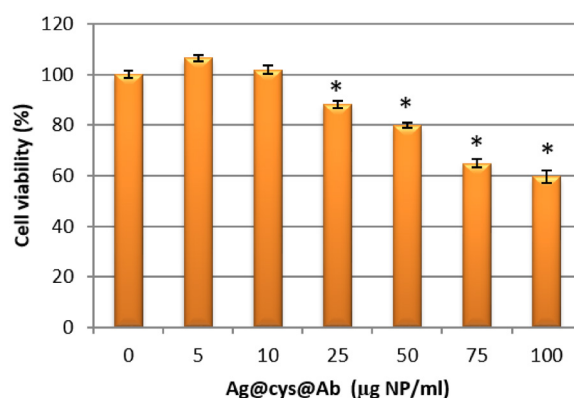The A431 cell line was chosen as suitable cellular model to study the biological behavior of Ag@cys@Ab nanoparticles.

Figure 8. Dose-dependent cytotoxicity of Ag@cys@Ab nanoparticles in A431 cells ($n = 3$; $*p < 0.05$).

A431 is an epidermoid carcinoma cell line widely employed as model target in the study of therapeutic approaches directed to EGFR, owing to the high EGFR expression reported for this cell line [55]. The cytotoxicity of Ag@cys@Ab nanoparticles was evaluated by resazurin-based *in vitro* toxicology assay following a 48 h exposure to the nanoparticles in concentrations ranging from 5 to 100 μg ml^{-1}. As expected, the deleterious effects of silver started to be observable (figure 8) only at typical doses previously described for other silver-based nanoparticles [56].

Importantly, concentrations below 50 μg nanoparticles per ml showed negligible effects on cell viability, thus rendering these particles useful for a number of biological applications [57]. For this reason, and in order to study the uptake of our targeted nanoparticles, we used a concentration of 10 μg ml^{-1} and analyzed via confocal microscopy the uptake of these particles after a 48 h incubation period. This analysis demonstrated that Ag@cys@Ab nanoparticles could be detected both by dark field (figure 9(a)) and fluorescence microscopies (figure 9(b)), suggesting feasibility of applications in theranostics.
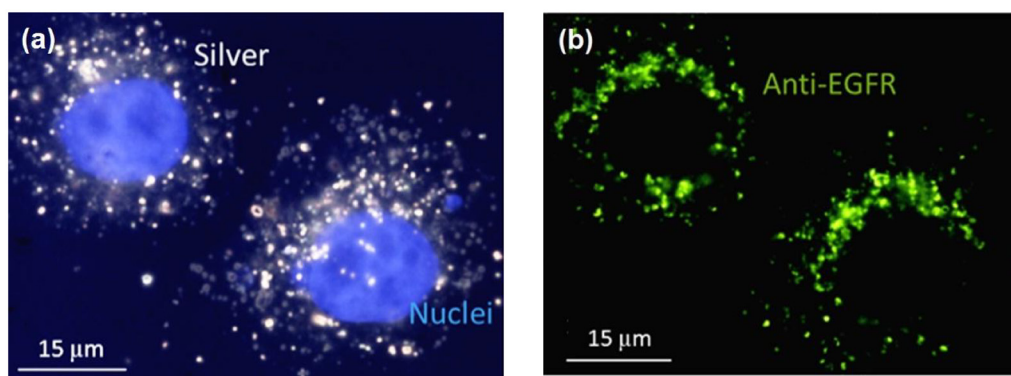
Adv. Nat. Sci.: Nanosci. Nanotechnol. **9** (2018) 015001

J M Oliva *et al*

Figure 9. Dark field and fluorescence microscopy images of A431 cells inoculated with Ag@cys@Ab nanoparticles. Nuclei were stained with Hoechst (blue) and monoclonal antibody was stained with AF488 (green). (a) Combined dark field and fluorescence images showing the position of nuclei (blue channel) and silver (dark field). (b) Fluorescence (green channel) image showing the position of the antibody conjugated to nanoparticles.

4. Conclusions

Our high-yield synthesis method produces highly concentrated small (12 nm) and narrow-sized silver nanoparticles, whose surfaces are highly decorated with terminal amine groups, with an S:Ag ratio as high as 0.76. These nanoparticles are stable over a remarkable range of pH values that includes physiological pH, with a zeta potential above 30 mV. Both the cysteamine to surface silver ratio and the total yield of the synthesis are remarkably higher than those described in the literature for other thiols. These features make our nanoparticles excellent candidates in drug delivery and gene transfection applications, as well as in biosensors and chemical sensors. Moreover, our synthesis method might be readily extended to obtain nanoparticles based on longer chain primary, secondary, ternary or even quaternary aminethiols, and could also be applied to other noble metal nanoparticles, providing an improved synthesis method over existing alternatives.

Additionally, we have coupled these nanoparticles to an antibody to EGFR, a 'hot' target due to its key role in the pathogenesis and progression of many solid tumors. These targeted nanoparticles have demonstrated both their labelling (fluorescence and dark field microscopies) and cytotoxic properties in A431 epidermoid carcinoma cells. Our results show the feasibility of using cysteamine-capped nanoparticles for therapeutic and diagnostic applications with a great potential in anticancer therapies due to the expected cytotoxic synergy between cysteamine and silver.

References

[1] Di Pietro P, Strano G, Zuccarello L and Satriano C 2016 *Curr. Top. Med. Chem.* **16** 3069
[2] Wei L, Lu J, Xu H, Patel A, Chen Z-S and Chen G 2015 *Drug Discov. Today* **20** 595
[3] Rycenga M, Cobley C M, Zeng J, Li W and Moran C H 2012 *Chem. Rev.* **111** 3669
[4] Zhang X-F, Liu Z-G, Shen W and Gurunathan S 2016 *Int. J. Mol. Sci.* **17** 1534
[5] Arvizo R R, Bhattacharyya S, Kudgus R A, Giri K, Bhattacharya R and Mukherjee P 2012 *Chem. Soc. Rev.* **41** 2943
[6] Doria G, Conde J, Veigas B, Giestas L, Almeida C, Assunção M, Rosa J and Baptista P V 2012 *Sensors* **12** 1657
[7] Azzazy H M E, Mansour M M H, Samir T M and Franco R 2012 *Clin. Chem. Lab. Med.* **50** 193
[8] Montes-García V, Pérez-Juste J, Pastoriza-Santos I and Liz-Marzán L M 2014 *Chem. Eur. J.* **20** 10874
[9] Comenge J *et al* 2016 *ACS Nano* **10** 7106
[10] Mahmoudi M, Amiri H, Shokrgozar M A, Sasanpour P, Rashidian B, Laurent S, Casula M F and Lascialfari A 2011 *Chem. Commun.* **47** 10404
[11] Bhattacharjee Y and Chakraborty A 2014 *ACS Sustain. Chem. Eng.* **2** 2149
[12] Wang L, Bi Y, Hou J, Li H, Xu Y, Wang B, Ding H and Ding L 2016 *Talanta* **160** 268
[13] Besouw M, Masereeuw R, Van Den Heuvel L and Levtchenko E 2013 *Drug Discov. Today* **18** 785
[14] Wu J *et al* 2016 *J. Biomed. Nanotechnol.* **12** 800
[15] Yu F *et al* 2016 *J. Biomed. Nanotechnol.* **12** 503
[16] Telli F C, Demir B, Barlas F B, Guler E, Timur S and Salman Y 2016 *RSC Adv.* **6** 105806
[17] Castilho M L, Hewitt K C and Raniero L 2017 *Sensors Actuators* B **240** 903
[18] Rahman M A *et al* 2012 *J. Control. Release* **159** 384
[19] Wu C, Shi L, Wu C, Guo D, Selke M and Wang X 2014 *Sci. China Chem.* **57** 1579
[20] Pandey S, Shah R, Mewada A, Thakur M, Oza G and Sharon M 2013 *J. Mater. Sci. Mater. Med.* **24** 1671
[21] Ghosh R, Singh L C, Shohet J M and Gunaratne P H 2013 *Biomaterials* **34** 807

Adv. Nat. Sci.: Nanosci. Nanotechnol. **9** (2018) 015001

J M Oliva *et al*

[22] Wu C, Shi L, Li Q, Jiang H, Selke M, Yan H and Wang X 2012 *Nanomed. Nanotechnol. Biol. Med.* **8** 860

[23] Soares J C, Shimizu F M, Soares A C, Caseli L, Ferreira J and Oliveira O N Jr 2015 *ACS Appl. Mater. Interfaces* **7** 11833

[24] Canbaz M C, Şimşek C S and Sezgintürk M K 2014 *Anal. Chim. Acta* **814** 31

[25] Xu P, Li J, Shi L, Selke M, Chen B and Wang X 2013 *Int. J. Nanomed.* **8** 3729

[26] Jv Y, Li B and Cao R 2010 *Chem. Commun.* **46** 8017

[27] Sharma A, Matharu Z, Sumana G, Solanki P R, Kim C G and Malhotra B D 2010 *Thin Solid Films* **519** 1213

[28] Jiang X, Yang M, Meng Y, Jiang W and Zhan J 2013 *ACS Appl. Mater. Interfaces* **5** 6902

[29] Luo Y, Xu J, Li Y, Gao H, Guo J, Shen F and Sun C 2015 *Food Control* **54** 7

[30] Ren S, Zhou F, Xu C and Li B 2015 *Gold Bull.* **48** 147

[31] Agoston R, Izake E L, Sivanesan A, Lott W B, Sillence M and Steel R 2016 *Nanomed. Nanotechnol. Biol. Med.* **12** 633

[32] Watanabe H, Kamikawa M, Nakagawa Y, Takahashi T and Ito A 1988 *Pathol. Int.* **38** 1285

[33] Inano H, Onoda M, Suzuki K, Kobayashi H and Wakabayashi K 2000 *Radiat. Res.* **153** 68

[34] Tatsuta M, Iishi H, Yamamura H, Baba M, Mikuni T and Taniguchi H 1988 *Int. J. Cancer* **41** 423

[35] Jeitner T M and Renton F J 2016 *Cancer Lett.* **103** 85

[36] Fujisawa T, Rubin B, Suzuki A, Patel P S, Gahl W A, Joshi B H and Puri R K 2012 *PLoS One* **7** e34437

[37] Wan X-M, Zheng F, Zhang L, Miao Y-Y, Man N and Wen L-P 2011 *Int. J. Cancer* **129** 1087

[38] Unak G, Ozkaya F, Ilker Medine E, Kozgus O, Sakarya S, Bekis R, Unak P and Timur S 2012 *Colloids Surf.* B **90** 217

[39] Pan Y-T, Smith C E, Kwok K S, Chen J, Kong H and Yang H 2015 *Chem. Commun.* **51** 14171

[40] Zheng Y, Tang Y, Bao Z, Wang H, Ren F, Guo M, Quan H and Jiang C 2015 *Int. J. Nanomed.* **10** 6435

[41] Ma L, Zou X and Chen W 2014 *J. Biomed. Nanotechnol.* **10** 1501

[42] Yao M, Ma L, Li L, Zhang J, Lim R X, Chen W and Zhang Y 2016 *J. Biomed. Nanotechnol.* **12** 1835

[43] Ong C, Lim J Z Z, Ng C-T, Li J J, Yung L-Y L and Bay B-H 2013 *Curr. Med. Chem.* **20** 772

[44] Fernandez-Montesinos R, Castillo P M, Klippstein R, Gonzalez-Rey E, Mejias J A, Zaderenko A P and Pozo D 2009 *Nanomedicine* **4** 919

[45] Michota A, Kudelski A and Bukowska J 2002 *Surf. Sci.* **502–3** 214

[46] Bayram S, Zahr O K and Blum A S 2015 *RSC Adv.* **5** 6553

[47] Yiu H H P, Bouffier L, Boldrin P, Long J, Claridge J B and Rosseinsky M J 2013 *Langmuir* **29** 11354

[48] Laban B, Vodnik V, Dramićanin M, Novaković M, Bibić N, Sovilj S P and Vasić V M 2014 *J. Phys. Chem.* C **118** 23393

[49] Castillo P M, Herrera J L, Fernandez-Montesinos R, Caro C, Zaderenko A P, Mejías J A and Pozo D 2008 *Nanomedicine* **3** 627

[50] Lee S Y, Noh J, Hara M and Lee H 2002 *Mol. Cryst. Liq. Cryst.* **377** 177

[51] Normanno N, De Luca A, Bianco C, Strizzi L, Mancino M, Maiello M R, Carotenuto A, De Feo G, Caponigro F and Salomon D S 2006 *Gene* **366** 2

[52] Goffin J R and Zbuk K 2016 *Clin. Ther.* **35** 1282

[53] Roskoski R 2014 *Pharmacol. Res.* **79** 34

[54] Yewale C, Baradia D, Vhora I, Patil S and Misra A 2013 *Biomaterials* **34** 8690

[55] Aguilera J R, Venegas V, Oliva J M, Sayagués M J, de Miguel M, Sánchez-Alcázar J A, Arévalo-Rodríguez M and Zaderenko A P 2016 *RSC Adv.* **6** 7279

[56] de Lima R, Seabra A B and Durán N 2012 *J. Appl. Toxicol.* **32** 867

[57] Chompoosor A, Saha K, Ghosh P S, MacArthy D J, Miranda O R, Zhu Z J, Arcaro K F and Rotello V M 2010 *Small* **6** 2246